external forcing with this time constant, but 1500 years is a reasonable time constant for an oscillation involving large-scale ocean circulation. This can be seen as follows. On the basis of a combination of atmospheric measurements and model simulations, it has been estimated that water vapor is being transported from the Atlantic Ocean to the Pacific and Indian oceans at the average rate of $0.25 \pm 0.10 \times 10^6$ m^3/s (*26*). Were this loss not compensated by salt export, the salinity of the Atlantic would increase by ~1 g/liter in 1500 years. Such an increase would have the same impact on the density of cold surface waters as a 5°C cooling would. Hence, one could envision that the export of salt required to balance its buildup in the Atlantic is cyclic rather than uniform.

One element in the debate regarding the consequences of the ongoing buildup of greenhouse gases has to do with distinguishing the contributions of natural and anthropogenic climate change. The post–Little Ice Age warming that occurred during the first half of the 20th century is comparable in magnitude to warming that occurred between 1975 and the present. During the former period, little buildup of greenhouse gases occurred. During the latter, an immense buildup has occurred. Those who call for action designed to stem the pace of the greenhouse buildup firmly believe that the warming during the latter part of the century was greenhouse driven. Those opposed to action would like to explain the entire warming as mainly natural. Thus, one of our tasks is to gain a better understanding of the Little Ice Age and its demise. If, as proposed here, changes in thermohaline are indeed involved, then a step toward this goal will have been taken.

References and Notes

1. K. A. Hughen *et al.*, *Nature* **391**, 65 (1998).
2. D. C. Barber *et al.*, *Nature* **400**, 344 (1999).
3. The conveyor refers to the large-scale circulation in the Atlantic Ocean. Warm waters in the upper 1500 m flow northward to the vicinity of Iceland. Winter cooling densifies this already salty water, permitting it to sink to the abyss. Once at depth, the water flows the length of the Atlantic and becomes entrained in the circum-Antarctic deep raceway. For details, see W. S. Broecker, *Oceanography* **4**, 79 (1991).
4. W. S. Broecker *et al.*, *J. Geophys. Res.* **103**, 15833 (1998).
5. S. Peacock, M. Visbeck, W. S. Broecker, in *Inverse Methods in Global Biogeochemical Cycles*, vol. 114 of *Geophysical Monograph Series* (American Geophysical Union, Washington, DC, in press).
6. E. Carmack, *Deep Sea Res. Oceanogr. Abstr.* **20**, 927 (1973); A. E. Gill, *Deep Sea Res. Oceanogr. Abstr.* **20**, 111 (1973); E. C. Carmack and T. D. Foster, *Deep Sea Res. Oceanogr. Abstr.* **22**, 77 (1975); T. D. Foster and J. H. Middleton, *J. Phys. Oceanogr.* **6**, 36 (1976); P. D. Killworth, *Deep Sea Res.* **24**, 427 (1977); R. L. Michel, *J. Geophys. Res.* **83**, 6192 (1978); R. F. Weiss, H. G. Ostlund, H. Craig, *Deep Sea Res. Part A* **26**, 1093 (1979); T. D. Foster and J. H. Middleton, *Deep Sea Res. Part A* **27**, 367 (1980); A. Foldvik, T. Gammelsrod, T. Torresen, in *Oceanology of the Antarctic Continental Shelf*, vol. 43 of *Antarctic Research Series*, S. S. Jacobs, Ed. (American Geophysical Union, Washington, DC, 1985), pp. 5–20; R. Bayer and P. Schlosser, *Mar. Chem.* **35**, 123 (1991); P. Schlosser, J. L. Bullister, R. Bayer, *Mar. Chem.* **35**, 97 (1991); A. L. Gordon, B. A. Huber, H. H. Hellmer, A. Ffield, *Science* **262** 95 (1993); E. Fahrbach *et al.*, *J. Mar. Res.* **53**, 515 (1995).
7. A. H. Orsi, G. C. Johnson, J. L. Bullister, *Prog. Oceanogr.* **43**, 55 (1999).
8. By ventilated deep water, we mean water that descended after contact with the atmosphere. As the PO_4^* value of Southern Ocean waters is reset mainly by the replenishment of O_2, it is important to exclude the contribution of older deep water entrained during the descent to the abyss. This is not to say that freshly ventilated waters are fully recharged with atmosphere gases. Measurements suggest that, in the Southern Ocean source regions, neither the O_2 nor the CFC content of the water reaches saturation. For both gases, the extent of saturation achieved appears to be ~70%. Orsi *et al.* (*7*) interpret the CFC-11 data to indicate 8 sverdrups of ventilation. On the basis of measurements of slope waters that had already entrained recirculated deep water, they assumed only 35% CFC-11 saturation. If the more reasonable 70% saturation value is adopted, then the flux of ventilated deep water drops to 4 sverdrups.
9. W. M. Smethie Jr. and R. A. Fine, *Deep Sea Res.*, in press.
10. J. M. Grove, *The Little Ice Age* (Methuen, New York, 1988).
11. E. A. Boyle, *Annu. Rev. Earth Planet. Sci.* **20**, 245 (1992); D. W. Lea and E. A. Boyle, *Nature* **338**, 751 (1989); J.-C. Duplessy *et al.*, *Paleoceanography* **3**, 343 (1988); D. W. Oppo and R. G. Fairbanks, *Earth Planet. Sci. Lett.* **86**, 1 (1987).
12. E. A. Boyle and L. D. Keigwin, *Nature* **330**, 35 (1987).
13. F. Gad, *The History of Greenland II, Earliest Times to 1700* (Hurst, London, 1970).
14. By ventilation time, we mean the time required for the production of new deep water to replace the water in the deep sea. Assuming a production rate of 30×10^6 m^3/s and that the volume of the deep sea is 60% of the total volume, this flushing time is 850 years.
15. M. E. Mann and R. S. Bradley, *Geophys. Res. Lett.* **26**, 759 (1999).
16. T. Sowers and M. Bender, *Science* **269**, 210 (1995).
17. R. B. Alley *et al.*, *Nature* **362**, 527 (1993).
18. D. A. Meese *et al.*, *Science* **266**, 1680 (1994).
19. W. S. Broecker, *Paleoceanography* **13**, 119 (1998).
20. T. F. Stocker, *Science* **282**, 61 (1998).
21. G. Clow, personal communication.
22. W. S. Broecker, *Science* **278**, 1582 (1997).
23. L. Keigwin, *Proc. Natl. Acad. Sci. U.S.A.*, in press.
24. G. Bond *et al.*, *Science* **278**, 1257 (1997).
25. R. A. Kerr, *Science* **284**, 2069 (1999).
26. F. Zaucker and W. S. Broecker, *J. Geophys. Res.* **97**, 2765 (1992).
27. P. Bergthórsson, *Joekull* **19**, 94 (1969).
28. B. Messerli, P. Messerli, C. Pfister, H. J. Zumbühl, *Arct. Alp. Res.* **10**, 247 (1978).

29. Discussions with L. Keigwin, B. Smethie, G. Clow, and G. Denton raised our interest in this subject. Financial support was provided by grant ATM 97-30546 from NSF. This is Lamont-Doherty Earth Observatory contribution number 5998.

12 July 1999; accepted 6 October 1999

Fault Slip Rates in the Modern New Madrid Seismic Zone

Karl Mueller,[1] Jocasta Champion,[1] Margaret Guccione,[2] Keith Kelson[3]

Structural and geomorphic analysis of late Holocene sediments in the Lake County region of the New Madrid seismic zone indicates that they are deformed by fault-related folding above the blind Reelfoot thrust fault. The widths of narrow kink bands exposed in trenches were used to model the Reelfoot scarp as a forelimb on a fault-bend fold; this, coupled with the age of folded sediment, yields a slip rate on the blind thrust of 6.1 ± 0.7 mm/year for the past 2300 ± 100 years. An alternative method used structural relief across the scarp and the estimated dip of the underlying blind thrust to calculate a slip rate of 4.8 ± 0.2 mm/year. Geometric relations suggest that the right lateral slip rate on the New Madrid seismic zone is 1.8 to 2.0 mm/year.

The clustered sequence of large-magnitude earthquakes that occurred within the New Madrid seismic zone (NMSZ) in 1811 and 1812 left no prominent evidence of surface fault rupture (Fig. 1A). There is, however, evidence for active uplift and surface deformation during these events across the Lake County Uplift (LCU), a compressive stepover in the mostly strike-slip NMSZ (*1–3*). An increasingly well-defined chronology of paleoearthquakes in the NMSZ has been developed through dating of liquefaction features (*4*) and syntectonic sediment derived by erosion of the Reelfoot scarp and infilled grabens (*5*). Determination of prehistoric earthquake magnitude in the NMSZ is difficult to define because (i) surface fault ruptures available for paleoseismic study have not been identified and (ii) methods used to define earthquake magnitude by paleoliquefaction features have not been readily calibrated by historic events.

We used fault-related fold theory (*6, 7*) to model the growth of the active LCU, based on trench exposures (*5*), microseismicity (*8*), high-resolution seismic reflection profiles (*9, 10*), and digital elevation models (Fig. 1B) (*11*). The purpose of our analysis is to determine the late Quaternary slip rate for the blind Reelfoot thrust fault by using fold geometry and structural relief. We also compared our estimated slip rates for the Reelfoot

[1]Department of Geological Sciences, University of Colorado, Boulder, CO 80309–0399, USA. [2]Department of Geology, University of Arkansas, Fayetteville, AR 72701, USA. [3]William Lettis and Associates, 1777 Botelho Drive, Suite 262, Walnut Creek, CA 94596, USA.

fault with recent geodetic surveys of the region (*12*, *13*) and estimated the timing of the onset of shortening across the thrust fault.

The LCU is made up of two active uplifts, Tiptonville Dome and Ridgely Ridge (Fig. 1B). Tiptonville Dome is a late Holocene uplift that stands 5 to 6 m above the surrounding Mississippi River floodplain. Strata deformed by the uplift include point bar, overbank, and channel fill deposits related to at least five separate abandoned Mississippi River meanders. The northern and western portions of Tiptonville Dome have been eroded by lateral migration of the Mississippi River (*14*). The eastern margin of the uplift is defined by the Reelfoot scarp, an east-facing fold limb (*5*). The deep structure of the LCU is defined by contemporary microseismicity (*8*), which illuminates a thrust fault dipping 34° west between 7- and 14-km depth (Fig. 2). Upward projection of this plane of microseismicity to the Reelfoot scarp suggests a fault that dips about 55° west between 7-km depth and the top of Paleozoic rocks at about 500-m depth (Fig. 2).

A line tracing of a depth-corrected high-resolution seismic reflection profile (*9*, *15*) located north of Reelfoot Lake shows the geometry of the Reelfoot monocline in the upper 500 to 600 m (Fig. 3B). Folded strata between the surface and ~100-m depth on the seismic profile typically dip less than 10°. Steeper dips are apparent between 200- and 400-m depth and reach 15° to 16° in the core of the fold limb. A closely spaced array of shallow soil borings (Fig. 3A) along the trace of the seismic line is interpreted to show two narrow monoclines whose steepest portions dip ~5° and 7.5° east and accommodate ~7 m of structural relief across the Reelfoot scarp. We were unable to determine the width of the two kink bands at this location because of a thick sand deposit situated between them. We interpret the sand body as either a point bar or extensional graben infill.

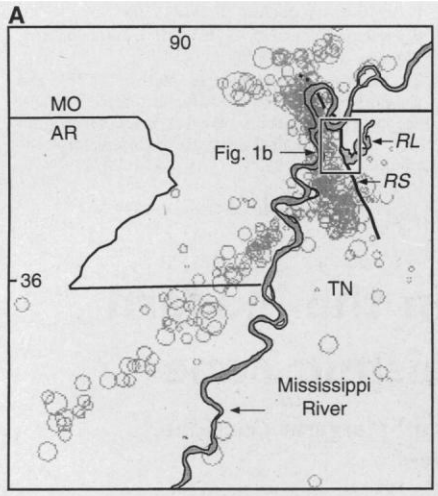

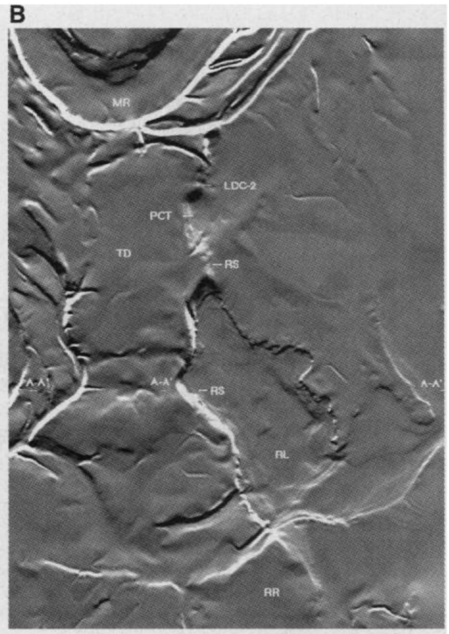

Fig. 1. (**A**) Location map showing seismicity for the period 1990 to 1999 for all events between magnitude 1.0 and 7.0. Note location of Reelfoot scarp (RS) relative to Reelfoot Lake (RL) and the NW-trending line of earthquakes that illuminate the blind Reelfoot thrust. The longer, NE-striking trend of seismicity coincides with the Cottonwood Grove fault. (**B**) Shaded relief map of the LCU constructed from a 1:62,500 scale topographic map with 5′ contours and a bathymetric map of Reelfoot Lake with 1′ contours acquired by the Tennessee Fish and Game Commission. The area of the image is 10.8 km by 15.8 km, with north at the top of the figure. The Reelfoot scarp (RS) is the narrow, east-facing feature that extends N-S through the center of the image. The depression east of the scarp is Reelfoot Lake (RL). Tiptonville Dome (TD) is the elongate, N-S–trending area of raised relief (~5 to 6 m at its northern end) located west of the Reelfoot scarp. The northernmost portion of Ridgely Ridge (RR) is in the lower center of the image. Other features include the modern channel of the Mississippi River (MR), the location of the seismic profile shown in Fig. 3B (LDC-2), the trench excavations at Proctor City (PCT), and the location of cross section A-A′ (Fig. 2).

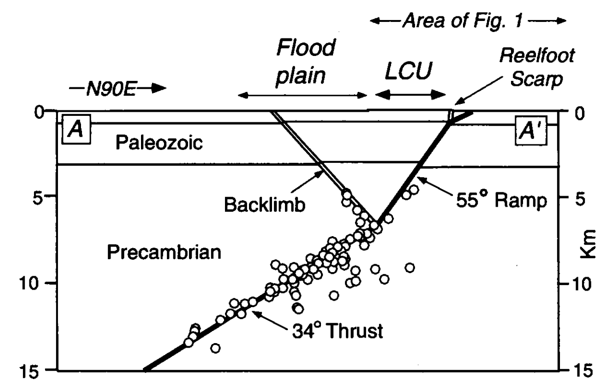

Fig. 2. Simplified cross section located along A-A′ of (*8*). See E-W extent of Fig. 1. Filled circles are relocated earthquakes (*8*). Note earthquakes that define both the shallow, west-dipping 34° thrust and the steeper 47° fold hinge that dips east. The fold hinge bisects the angle formed by the flatter 34° and steeper 55° thrust ramps. The Reelfoot scarp is interpreted as a forelimb in a nascent fault-bend fold, where the thrust flattens abruptly upward at ~650-m depth. Relief across the LCU is only ~37 m and barely apparent on the section.

Trenches and pits were excavated across the scarp, expanding work at an existing site (Proctor City) (*5*) 900 m south of the seismic line and soil boring profile (Fig. 1B). Excavations across the scarp at Proctor City indicate three narrow, east-facing monoclines that dip between ~5° and 16° and accommodate 9 m of structural relief (Fig. 4A). The east-dipping monoclines are separated by strata that dip ~2° west. The three narrow monoclines that make up the Reelfoot scarp at the trench site (Fig. 4C) have steep segments that are 12.3, 15.0, and 14.3 m wide (*16*). North-striking normal faults and graben exposed in trench excavations imply that extension is an important deformation mechanism that accompanies bending (*5*).

We considered a number of folding mechanisms for Tiptonville Dome including fault-bend and fault-propagation folds, a wedge-thrust structure, and elastic folding above a dislocation. Most of the near-surface deformation above 500-m depth can be fit by a fault-bend fold model in which the Reelfoot scarp develops above two or three abrupt, convex-upward bends at the top of a thrust ramp interpreted to dip ~55° west [for example, see (*7*)]. We interpret Tiptonville Dome to be uplifted above the steep 55° thrust ramp (Fig. 2), similar to an existing model (*17*). The narrow, east-dipping band of microseismicity from 4.5- to 6.5-km depth is, however, interpreted to record strain produced by folding across an active hinge zone pinned to the base of the steep ramp. This band of seismicity dips 47° east and defines an interlimb bisector between a ramp dipping 55° west and the deeper, 34° west-dipping thrust defined by seismicity (Fig. 2) (*8*). This is similar to a fold hinge illuminated by earthquakes in the Santa Barbara Channel in offshore southern California (*18*). However, in our model, these small earthquakes occur in basement rocks where we do not expect them to form in response to flexural slip unless Precambrian rocks here contain a strongly developed, flat-lying foliation. Our cross section is an alternative to an existing model (*17*), in which the 47° east-dipping band of seismicity is interpreted as a back thrust. The orientation of the east-dipping band of seismicity is consistent with fault-bend fold theory, in which active

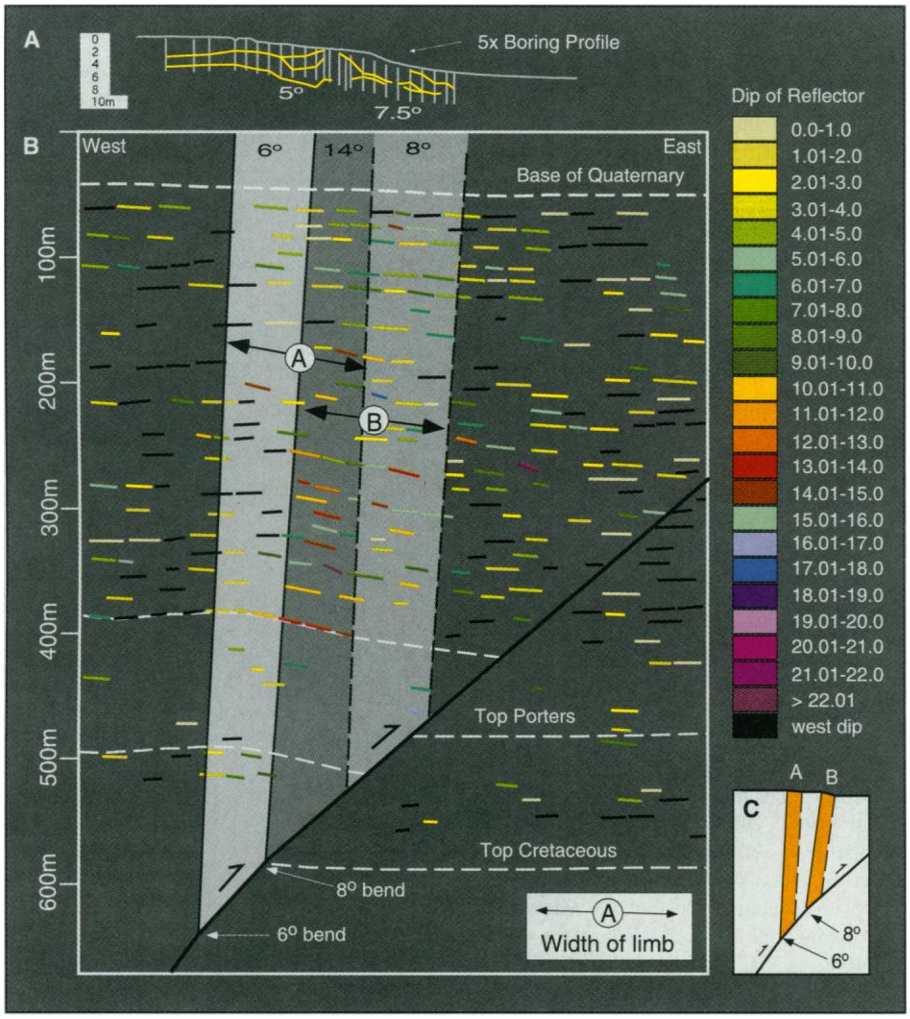

Fig. 3. (**A**) Vertically exaggerated (5×) profile of folded shallow strata defined by continuously cored soil borings located along trace of underlying seismic line. Lines are readily identifiable stratigraphic contacts. Note 5° and 7.5° east-dipping panels. The central part of the profile includes a point bar deposit or extensional graben that obscures the geometry of the kink bands. (**B**) Tracing of a depth-migrated seismic line (LDC-2) (*9*). The dip of the reflectors corresponds to color scale. The profile is interpreted to illustrate two overlapping kink bands that are each ~100 m wide. Note 6°, 14°, and 8° dip panels predicted by the fault-bend fold model. The middle panel is interpreted to be the sum of overlapped 6° and 8° panels. We interpret differences in reflector geometry from our fault-bend fold model to be related to both the effects of a broad wavelength fold apparent in other seismic sections (*10*) or from structures that existed before the late Quaternary history of shortening across the LCU. (**C**) Simplified cross section of kink bands formed above two bends that do not overlap. Compare figure with trench logs (Fig. 4), where kink bands deform very young strata. Overlapping panels are only apparent on seismic reflection profiles in older Tertiary and Cretaceous strata. The near-surface folds record narrower limbs produced by fault slip for only the past 2.3 ka, the age of fluvial strata in the trench that predate evidence of scarp-derived colluvium. For deposition in the Mississippi River floodplain, deformation is "reset" or "zeroed" after channel meanders erode through the uplifted area and deposit horizontal sediment in their wake.

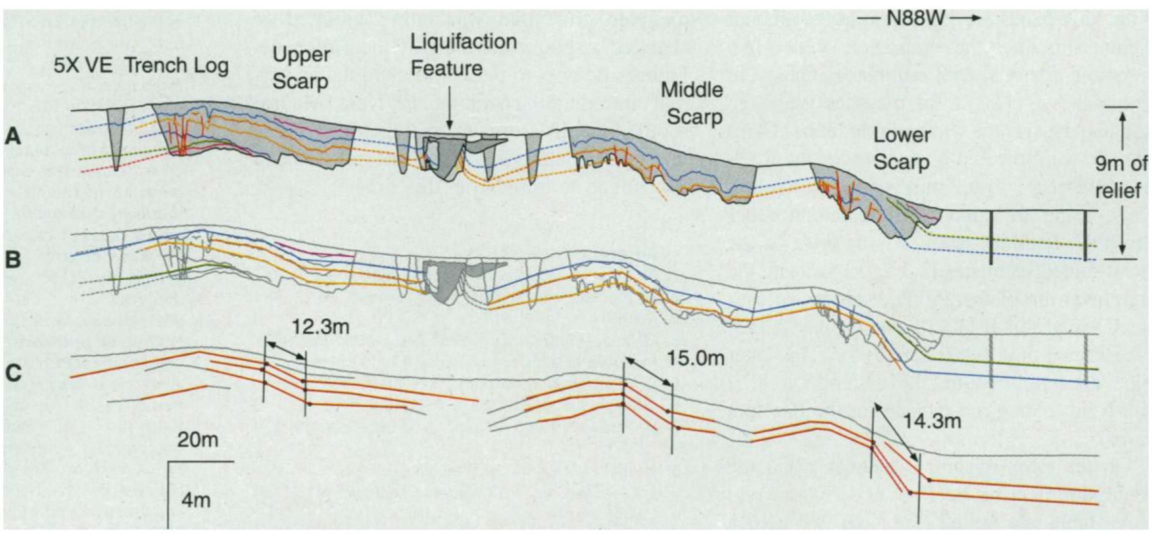

Fig. 4. (**A**) Logs of trench excavations and pits located across the Reelfoot scarp at Proctor City site (PCT on Fig. 1). Eastern trench log over lowest scarp from previous study (*5*). Solid lines are readily identifiable stratigraphic contacts, whereas dashed line are correlations between excavations. A very large liquefaction feature is shown between upper and middle scarp. The lower and middle scarps are continuous northward to the two scarps at site LDC-2, shown on Fig. 3, A and B. (**B**) Simplified stratigraphic contacts defined by correlation across liquefaction features, which are areas of local collapse related to expulsion of liquefied sand. (**C**) Kink bands used in slip rate calculations. Gray lines are equivalent to colored lines in (B). The steepest portions of the fold limbs are used to define limb width. Limbs are measured parallel to bedding; width is shown in meters above each scarp. Note the relatively narrow width of the kink bands in the trench excavations (<15 m) in comparison with those defined on the seismic reflection profile (~100 m) (Fig. 3B). Axial surfaces are defined by locations of projected beds at multiple stratigraphic intervals (that is, small black circles).

axial surfaces bisect limbs whose geometry is governed by the change in dip of the fault segments.

The geometry of the thrust above 550-m depth (that is, above the steeply dipping 55° ramp) is poorly defined by available subsurface data. Continuous reflectors of folded strata are not apparent on seismic reflection profiles at the appropriate depth range (*9*, *10*), and there is little or no microseismicity above 4.5-km depth (*8*). Discontinuous reflectors of Eocene and Paleocene strata do, however (*9*, *10*), permit an interpretation of a thrust fault that is a more flat-lying continuation of the 55° ramp. The decrease in dip of the thrust fault from the deeper 55° segment to the shallower segment that we interpret in the upper 600 m (that is, from west to east) is consistent with growth of the Reelfoot scarp as an east-dipping forelimb in a fault-bend fold (Fig. 2). The sum of the dips of the two kink bands exposed in the boring profile (~12.5°) (Fig. 3A) is also consistent with multibend fault-bend folding (*19*); this value is about the same as the steepest dips defined in the depth-corrected seismic line (~13° to 14°, Fig. 3B) where two kink bands are interpreted to overlap and sum (*7*). Extensional features exposed in trench excavations along the Reelfoot scarp (*5*) support the interpretation of the scarp as a forelimb, where the hanging-wall block collapses onto a flatter fault segment. The similarity in width of the three kink bands (12.3, 15.0, and 14.3 m) is also broadly consistent with fault-bend fold theory (*6*), in which similar amounts of fault displacement produce fold limbs of equal width at different points on the same fault.

We used the width of kink bands exposed in trench excavations at the Proctor City site to determine the slip rate on the underlying blind thrust. On the basis of our interpretation of the Reelfoot scarp as a fault-bend fold, the widths of the kink bands are equivalent to the amount of fault slip since the strata were folded (*6*). Given the age of fluvial sediments exposed in the trenches (*5*) [2.3 ± 0.1 thousand years ago (ka)] and the average width of fold limbs (14 m) (Fig. 4), we estimated a slip rate for the Reelfoot fault of 6.1 ± 0.7 mm/year (*20*). Alternatively, using the amount of structural relief across the Reelfoot scarp (9.1 m) (Fig. 4), the age of folded sediments (2.3 ± 0.1 ka), and the interpreted dip of the 55° fault ramp, we estimated a total slip of 11.1 m over the past 2.3 ka, or a slip rate of 4.8 ± 0.2 mm/year. This latter value does not require the assumption of a fault-bend folding mechanism for the Reelfoot scarp.

On the basis of simple geometry and the assumption that the Reelfoot and Cottonwood Grove faults are linked (Fig. 1A), we used a vector analysis to calculate a slip rate for the southern part of the NMSZ. Using the slip rates on the Reelfoot thrust derived above, we estimated a right lateral slip rate for the Cottonwood Grove fault of 1.8 to 2.2 mm/year (*21*). Our values for the Cottonwood Grove fault are within the range of values for the slip rate interpreted from a recent geodetic survey that used highly stable monuments throughout Lake County (*12*). In this analysis, local network sites yield a best fit of 0.7 ± 2.5 mm/year. Our independent analysis results in rates that lie within the error analysis provided by the geodetic survey, although in the more rapid range of possible values.

The onset of shortening across the LCU can be calculated if the slip rate defined by our analysis is assumed to be constant since movement on the Reelfoot fault was initiated. We used the structural solution shown on the depth-migrated seismic reflection profile (Fig. 3B) to define the total width of fault-bend fold limbs in the Reelfoot monocline as ~100 m. Given a rate of limb widening of 6.1 ± 0.7 mm/year, this yields an onset of shortening at about 16.4 ka. Using an alternative method, we measured the amount of total structural relief (37 m) seen on the depth-migrated seismic profile (Fig. 3), an uplift rate of 4.0 mm/year (derived from the amount of relief in the trench excavations and the age of folded late Holocene sediments), and a 55° dipping thrust to define the onset of shortening as 9.3 ka. Either calculation supports earlier suggestions that the NMSZ is a young, transient feature, which has not accumulated substantial long-term strain (*22*). We favor the younger value (9.3 ka) because of uncertainties inherent in accurately locating the edges of gently dipping kink bands at depth on the seismic profile.

We do not attempt to ascribe a mechanism for the modern reactivation of the NMSZ as an active source of hazardous earthquakes. Our estimates of the onset of uplift in the restraining bend do, however, point to a rheological or stress-related condition in the seismogenic crust that was either initiated or changed at about the start of the Holocene. Future attempts to unlock the enigma of current intraplate seismicity in New Madrid should benefit from an examination of the timing of loading or heat flow phenomena that might be initiated at this time.

References and Notes

1. M. L. Fuller, *U.S. Geol. Surv. Bull.* **494**, 119 (1912).
2. D. Merritts and T. Hesterberg, *Science* **265**, 1081 (1994).
3. D. Russ, *U.S. Geol. Surv. Prof. Pap.* **1236**, 94 (1982).
4. M. Tuttle *et al.*, *Geoarcheology* **11**, 451 (1996).
5. K. Kelson *et al.*, *J. Geophys. Res.* **101**, 6151 (1996).
6. J. Suppe, *Am. J. Sci.* **283**, 684 (1983).
7. D. Medwedeff and J. Suppe, *J. Struct. Geol.* **19**, 279 (1997).
8. J. Pujol *et al.*, *Eng. Geol.* **46**, 21 (1997).
9. J. L. Sexton and P. B. Jones, *Geophysics* **31**, 1760 (1986).
10. J. K. Odum *et al.*, *Geol. Soc. Am. Bull.* **110**, 149 (1998).
11. The digital elevation model (DEM) was created from a digitized 1939 U.S. Army Corps of Engineers 1:62,500 scale topographic map with a 5′ contour interval. The resulting DEM was manipulated in ENVI to produce the shaded relief map seen in Fig. 1B.
12. A. Newman *et al.*, *Science* **284**, 619 (1999).
13. S. Kerkela *et al.*, *Eos* **79** (Fall Meet. Suppl.), F201 (1998).
14. R. T. Saucier, *Geomorphology and Quaternary Geologic History of the Lower Mississippi Valley*, prepared for the President, Mississippi River Commission (U.S. Army Waterways Experiment Station, Vicksburg, MS, 1994), vol. 2.
15. We depth-corrected profile LDC-2 of (9) by tying prominent reflectors with high impedance contrast (for example, base Quaternary, top Porters Creek Clay, and top Cretaceous) to a nearby well, the Kate Wright No. 1, located less than 100 m from the western endpoint of the seismic line. Short straight segments of reflectors were traced from the depth-migrated section; these segments were then depth-corrected with the known depth of correlative stratigraphic units in the nearby well.
16. We measured limb width in the three trench excavations by projecting the steepest portion of the east-facing fold limbs to their intersections with projections of adjacent flat-lying or gently west-dipping strata (Fig. 4C). We ignored large collapse features and sandblows in these projections.
17. J. Purser and R. Van Arsdale, *Bull. Seismol. Soc. Am.* **88**, 1204 (1998).
18. J. Shaw and J. Suppe, *Geol. Soc. Am. Bull.* **106**, 607 (1994).
19. For transferal of fault slip across multibend fault-bend folds, we argue that the minimum total change in fault trajectory (that is, the change in fault dip measured across all bends) is defined by the sum of the steepest portions of individual kink bands. This is for the case in which the amount of fault slip exceeds the spacing between adjacent active axial surfaces. We do not suggest that fault-bend folds are perfectly angular and completely reflect changes in fault trajectory (for example, fault bends). Increase in the radii of curvature of fault-bend folds as they propagate upward through sedimentary rocks depends on both the rigidity of folded sedimentary beds and the spacing of flexural slip faults that accommodate kink-band migration. We argue that our assumption of fault-related folding is a valid deformation mechanism for the Reelfoot scarp because the bend in the thrust occurs at a shallow depth (that is, 500 m) and because overlying Tertiary sediments are well bedded. We modeled the fault-bend fold as made up of two bends where it is imaged by the seismic reflection profile and boring profile and three bends where the trench excavations were completed. These bends are apparent at the surface as smaller scarps in the larger Reelfoot "scarp" but are not resolvable on the shaded relief image shown in Fig. 1B.
20. For the slip rate defined by the limb widths measured in the trenches, uncertainty is calculated as standard error, which takes into account both the variance in the measurements and the uncertainty in the radiocarbon age (for example, 0.7 mm/year). For the slip rate defined by structural relief and fault dip, uncertainty depends only on the uncertainty in the radiocarbon age because only one measurement, 9.1 m of uplift, is used (for example, 0.2 mm/year). Our attempt to fit the dip of the 55° fault ramp to the seismicity data and the location of the Reelfoot scarp can be varied by as much as 5° of dip. For a fault dip of 50°, we determined a slip rate of 5.2 mm/year; for a fault dip of 60°, we determined a rate of 4.6 mm/year.
21. We used a slip vector on the blind thrust fault of 55°, N88°W, perpendicular to the strike of the Reelfoot scarp at the trench site. The rate of horizontal shortening perpendicular to the strike of the Reelfoot thrust is equivalent to the cosine of the dip of the thrust (that is, 55°) multiplied by the slip rate. For the two slip rates we determined, this yields rates of 2.8 or 3.4 mm/year. The cosine of the horizontal angle between the trend of the slip vector on the thrust and the strike of the Cottonwood Grove fault (that is, 50°) is then multiplied by the rate of horizontal shortening across the thrust to yield the slip rate on the regional strike-slip system of 1.8 or 2.2 mm/year.
22. E. S. Schweig and M. A. Ellis, *Science* **264**, 1308 (1994).

6 April 1999; accepted 4 October 1999

LINKED CITATIONS

You have printed the following article:

Fault Slip Rates in the Modern New Madrid Seismic Zone
Karl Mueller; Jocasta Champion; Margaret Guccione; Keith Kelson
Science, New Series, Vol. 286, No. 5442. (Nov. 5, 1999), pp. 1135-1138.
Stable URL:
http://links.jstor.org/sici?sici=0036-8075%2819991105%293%3A286%3A5442%3C1135%3AFSRITM%3E2.0.CO%3B2-J

This article references the following linked citations:

References and Notes

[2] **Stream Networks and Long-Term Surface Uplift in the New Madrid Seismic Zone**
Dorothy Merritts; Tim Hesterberg
Science, New Series, Vol. 265, No. 5175. (Aug. 19, 1994), pp. 1081-1084.
Stable URL:
http://links.jstor.org/sici?sici=0036-8075%2819940819%293%3A265%3A5175%3C1081%3ASNALSU%3E2.0.CO%3B2-V

[12] **Slow Deformation and Lower Seismic Hazard at the New Madrid Seismic Zone**
Andrew Newman; Seth Stein; John Weber; Joseph Engeln; Ailin Mao; Timothy Dixon
Science, New Series, Vol. 284, No. 5414. (Apr. 23, 1999), pp. 619-621.
Stable URL:
http://links.jstor.org/sici?sici=0036-8075%2819990423%293%3A284%3A5414%3C619%3ASDALSH%3E2.0.CO%3B2-G

[22] **Reconciling Short Recurrence Intervals With Minor Deformation in the New Madrid Seismic Zone**
Eugene S. Schweig; Michael A. Ellis
Science, New Series, Vol. 264, No. 5163. (May 27, 1994), pp. 1308-1311.
Stable URL:
http://links.jstor.org/sici?sici=0036-8075%2819940527%293%3A264%3A5163%3C1308%3ARSRIWM%3E2.0.CO%3B2-G

NOTE: *The reference numbering from the original has been maintained in this citation list.*